Solution Structure, Backbone Dynamics, and Interaction with Cdc42 of *Salmonella* Guanine Nucleotide Exchange Factor SopE2[†,‡]

Christopher Williams,[§,||] Edouard E. Galyov,[⊥] and Stefan Bagby*[,§]

Department of Biology and Biochemistry, University of Bath, Bath BA2 7AY, U.K., and Division of Environmental Microbiology, Institute for Animal Health, Compton Laboratory, Berkshire RG20 7NN, U.K.

Received May 7, 2004; Revised Manuscript Received July 13, 2004

ABSTRACT: SopE and SopE2 are delivered by the *Salmonella* type III secretion system into eukaryotic cells to promote cell invasion. SopE and SopE2 are potent guanine nucleotide exchange factors (GEFs) for Rho GTPases Cdc42 and Rac1 and constitute a novel class of Rho GEFs. Although the sequence of SopE-like GEFs is not at all homologous to those of the Dbl homology domain-containing eukaryotic GEFs, the mechanism of nucleotide release seems to have significant similarities. We have determined the solution structure of the catalytic domain (residues 69−240) of SopE2, showing that $SopE2_{69-240}$ comprises two three-helix bundles (α1α4α5 and α2α3α6) arranged in a Λ shape. Compared to the crystal structure of $SopE_{78-240}$ in complex with Cdc42, $SopE2_{69-240}$ exhibits a less open Λ shape due to movement of $SopE_{78-240}$ helices α2 and α5 to accommodate binding to the Cdc42 switch regions. In an NMR titration to investigate the $SopE2_{69-240}$−Cdc42 interaction, the $SopE2_{69-240}$ residues affected by binding Cdc42 were very similar to the $SopE_{78-240}$ residues that contact Cdc42 in the $SopE_{78-240}$−Cdc42 complex. Analysis of the backbone ^{15}N dynamics of $SopE2_{69-240}$ revealed flexibility in residues that link the two three-helix bundles, including the α3−α4 linker that incorporates a β-hairpin and the catalytic loop, and the α5−α6 loop, and flexibility in residues involved in interaction with Cdc42. Together, these observations provide experimental evidence of a previously proposed mechanism of GEF-mediated nucleotide exchange based on the Rac1−Tiam1 complex structure, with SopE/E2 flexibility, particularly in the interbundle loops, enabling conformational rearrangements of the nucleotide binding region of Cdc42 through an induced fit type of binding. Such flexibility in SopE/E2 may also facilitate interaction through adaptive binding with alternative target proteins such as Rab5, allograft inflammatory factor 1, and apolipoprotein A-1.

Salmonella enterica are facultative intracellular enteric pathogens that cause a broad range of diseases in a variety of vertebrates. A crucial component in host cell invasion by *Salmonella* is the specialized type III secretion system (TTSS),[1] a common mechanism by which Gram-negative pathogenic and symbiotic animal and plant bacteria deliver a battery of effector proteins into host cells (*1*). Among other effects, *Salmonella* virulence proteins delivered by this system cause pronounced membrane ruffling and actin cytoskeleton rearrangements at the point of contact between the bacterium and host cell, leading to bacterial internalization. *Salmonella* invasion of host cells is dependent on host cell Rho GTPases Cdc42 and Rac1 (*2*).

Rho GTPases, a family of monomeric GTP-binding proteins, are key regulators for a wide range of cellular responses, including cytoskeletal reorganization, focal adhesions, motility, membrane ruffling, cytokinesis, cell aggregation, cell−cell adhesion, gene expression, mitogenic signaling, and malignant transformation (*3*−*6*). Rho GTPases act as molecular switches, cycling between GDP-bound (inactive) and GTP-bound (active) conformations. All GTPases have a similar core fold consisting of a mixed six-stranded β-sheet and five α-helices located on either side. Two highly flexible regions, termed switch I and switch II, exhibit the major conformational differences between GDP-bound and GTP-bound forms and define the on and off states of GTPases. The conserved P-loop (phosphate binding loop) in the binding pocket is involved in stabilizing the active conformation. Mg^{2+} is essential for GTPase function and structure, contributing to the tight binding of the nucleotides

[†] This work was supported at the University of Bath by The Wellcome Trust (Grant 060998) and at the Institute for Animal Health by BBSRC. The Wellcome Trust is acknowledged for purchase of the 600 MHz NMR spectrometer (Grant 051902) used in this study. C.W. was supported by a Ph.D. studentship from EPSRC.

[‡] Coordinates of the 20 lowest-energy structures and the structure closest to the mean have been deposited in the Protein Data Bank as entries 1R6E and 1R9K, respectively.

* To whom correspondence should be addressed: Dr. Stefan Bagby, Department of Biology & Biochemistry, University of Bath, Bath BA2 7AY, UK. Tel: +44 (0)1225 386436. Fax: +44 (0)1225 386779. Email: bsssb@bath.ac.uk.

[§] University of Bath.

[||] Present address: School of Chemistry, University of Bristol, Cantock's Close, Bristol BS8 1TS, U.K.

[⊥] Compton Laboratory.

[1] Abbreviations: DH, Dbl homology; DTT, dithiothreitol; EDTA, ethylenediaminetetraacetic acid; GdnHCl, guanidine hydrochloride; GEF, guanine nucleotide exchange factor; GST, glutathione *S*-transferase; HEPES, 4-(2-hydroxyethyl)piperazine-1-ethanesulfonic acid; HSQC, heteronuclear single-quantum coherence; IPTG, isopropyl β-D-thiogalactoside; NMR, nuclear magnetic resonance; NOE, nuclear Overhauser effect; PH, pleckstrin homology; rmsd, root-mean-square deviation; SCV, *Salmonella*-containing vesicle; Tris, tris(hydroxymethyl)aminomethane; TTS, type III secretion; TTSS, type III secretion system.

10.1021/bi0490744 CCC: $27.50
Published on Web 08/28/2004

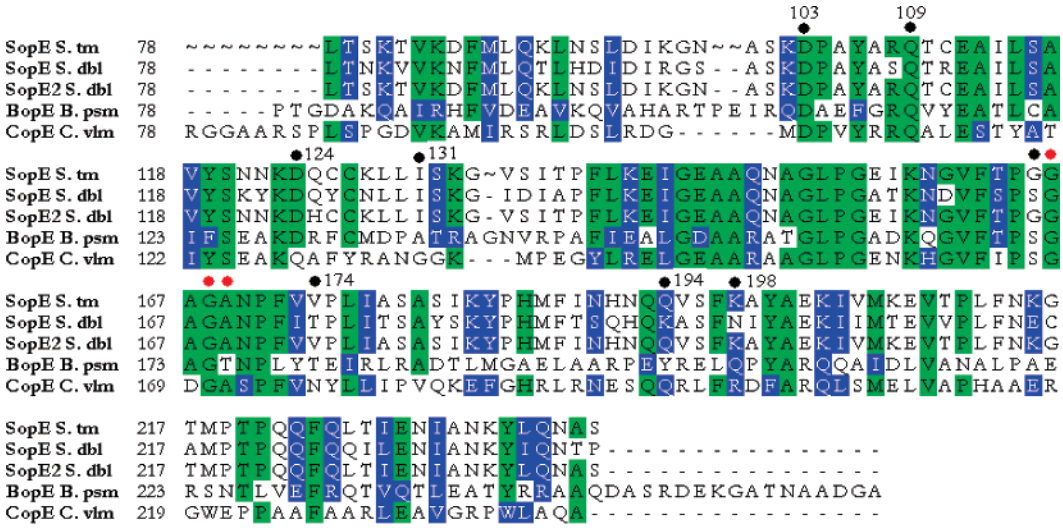

FIGURE 1: Family of SopE-like proteins. Alignment of the catalytic domains of *S. enterica* serovar Typhimurium SopE (GenBank accession number AF043239), *S.* Dublin SopE (GenBank accession number AF006949), *S.* Dublin SopE2 (GenBank accession number Q9KIZ2), *Burkholderia pseudomallei* BopE (GenBank accession number NC_002930), and *C. violaceum* CopE (GenBank accession number AAQ57975) performed using ClustalW. Residues conserved in at least four of the sequences are highlighted in green and conservatively substituted residues in blue. SopE residues that interact with Cdc42 in the $SopE_{78-240}$−Cdc42 crystal structure are denoted with black filled circles and a residue number, except Cdc42-interacting residues from the catalytic GAGA motif (residues 166−169 in SopE and SopE2) which are denoted with red filled circles without a residue number (*24*). SopE induces the release of nucleotides from Cdc42 by inserting its GAGA loop between the switch regions of Cdc42, apparently pushing switch I aside and pulling switch II toward the GAGA loop (*24*).

in both the GDP and GTP conformations. As the intrinsic rates of nucleotide release and GTP hydrolysis are slow, interconversion between these forms depends on accessory effectors. GTPase activation is tightly regulated by guanine nucleotide exchange factors (GEFs) which stimulate the dissociation of GDP and its subsequent exchange for GTP by inducing structural changes in the nucleotide binding site in response to upstream signals (*5*, *7*−*9*). The best characterized eukaryotic Rho GEFs contain a catalytic Dbl homology (DH) domain followed by a pleckstrin homology (PH) domain for membrane association (*10*). The structures of GEF−Rho GTPase complexes have revealed that the DH domain binds to the switch regions of the GTPase and alters their conformation, ultimately destabilizing nucleotide and magnesium ion interactions (*11*−*13*). The altered conformation induced upon binding also results in the intrusion of GEF residues into the nucleotide binding site, further destabilizing nucleotide binding.

S. enterica serovar Typhimurium (*S.* Typhimurium) invasion of host cells depends on at least three type III secreted effector proteins: SopE (*14*) (present only in some strains), SopE2 (*15*, *16*), and SopB, an inositol phosphatase (*17*, *18*). SopE and SopE2 are GEFs for the Rho GTPases Cdc42 and Rac1 (*19*−*21*). Unlike eukaryotic Rho GEFs, however, SopE and SopE2 do not contain a DH domain and constitute a distinct group of Rho GEFs. This group also includes the effector protein BopE from *Burkholderia* spp. (*22*) and a putative protein from the Gram-negative opportunistic human pathogen *Chromobacterium violaceum* (*23*) (Figure 1). Although the sequences of SopE-like GEFs are not at all homologous with those of the eukaryotic GEFs and lack DH and PH domains, they exhibit nucleotide exchange rates similar to those of eukaryotic GEFs (*19*, *20*). The crystal structure of the SopE−Cdc42 complex showed that SopE has a unique tertiary fold, and that although SopE employs residues different from those of eukaryotic Rho GEFs to bind and induce catalysis, the conformations of the switch I and II regions of Cdc42 resemble those in DH GEF−Rho GTPase complexes (*24*). Additionally, a number of SopE residues involved in stabilizing the rearranged nucleotide binding region form polar contacts with Cdc42 residues in an analogous fashion with residues in DH GEFs.

Although the sequences of SopE and SopE2 are 69% identical (Figure 1), they specifically activate different sets of Rho GTPase signaling cascades, allowing *Salmonella* to precisely manipulate host cell physiology. *In vitro* guanine nucleotide exchange assays demonstrated that *S.* Typhimurium $SopE_{78-240}$ acts as a GEF equally efficiently for both Rac1 and Cdc42, whereas *S.* Typhimurium $SopE2_{69-240}$ is a more efficient GEF for Cdc42 than SopE, but is less active on Rac1 (*20*). SopE can also act as a GEF for Rab5 and can mediate its recruitment in the GTP-bound form to *Salmonella*-containing vesicles (SCVs). Rab5 is a key regulator of the early endocytic compartments, and recruitment of the active form to the SCV is thought to block specific membrane fusion events following host cell invasion (*25*).

Although the basis of substrate specificity has been elucidated for a number of DH GEFs, the lack of any sequence homology between the SopE-like GEFs and DH GEFs makes it difficult to predict the molecular basis of recognition for the SopE-like GEFs. To develop further insights into the behavior of this novel family of GEFs, the NMR solution structure of the catalytic domain (residues 69−240) of non-DH GEF SopE2 from *S. enterica* serovar Dublin (*S.* Dublin) has been determined and compared to the crystal structure of the *S.* Typhimurium SopE catalytic domain (residues 78−240) in complex with Cdc42 (*24*). These comparisons reveal some differences in the tertiary structures of $SopE2_{69-240}$ and Cdc42-bound $SopE_{78-240}$. To explore the interaction of SopE2 with its cellular targets in solution, we mapped the binding of Cdc42 to $SopE2_{69-240}$ and found that the $SopE2_{69-240}$ residues affected by binding Cdc42 are similar to the $SopE_{78-240}$ residues that interact with Cdc42 in the $SopE_{78-240}$−Cdc42 complex crystal structure, but with

the notable addition of residues in helix α6. Complementary information provided by backbone ^{15}N relaxation analysis reveals flexibility in SopE2$_{69-240}$ that is compatible with SopE2 engagement of Cdc42 through an induced fit mechanism.

MATERIALS AND METHODS

Sample Preparation. NMR samples of the *S.* Dublin SopE2 catalytic domain (residues 69−240) were prepared as previously described (*26*). Typically, NMR samples were approximately 300 μL in volume in a 5 mm diameter Shigemi tube. Samples were degassed and sealed under a nitrogen atmosphere at room temperature. Unlabeled SopE2$_{69-240}$ samples in 99.96% D_2O were prepared in a similar manner in 20 mM Tris-d_{11}-DCl (pH 7.0) and 1 mM d_{10}-DTT. Protein concentrations were determined by measuring the absorption at 280 nm in 6 M GdnHCl, and were in the range of 1.0−1.5 mM, unless otherwise stated.

NMR Spectroscopy. All NMR data were acquired at 25 °C on a Varian Unity INOVA spectrometer operating at a nominal proton frequency of 600 MHz, using a triple-resonance 5 mm probe equipped with *z*-axis pulsed field gradients. NMR data were processed using the NMRPipe/NMRDraw software suite (*27*) and analyzed using the SPARKY assignment program (*28*).

Sequence-specific backbone and side chain ^{1}H, ^{13}C, and ^{15}N resonance assignments of SopE2$_{69-240}$ have been reported previously (BioMagResBank entry 5701) (*26*). NOE distance restraints were obtained by analysis of ^{1}H−^{1}H two-dimensional (2D) NOESY (*29*) (100 and 175 ms mixing times), ^{15}N NOESY-HSQC (50, 100, and 150 ms mixing times) (*30*), and simultaneous three-dimensional (3D) ^{15}N/^{13}C-edited NOESY (*31*) (100 ms mixing time) spectra.

Structure Calculation. Each NOE was assigned to one of four restraint distances based on the peak intensity: 1.8−2.8, 1.8−3.3, 1.8−5.0, and 1.8−6.0 Å, corresponding to strong, medium, weak, and very weak NOEs, respectively. Distances involving methyl groups, aromatic ring protons, and non-stereospecifically assigned methylene protons were represented as a $(\sum r^{-6})^{-1/6}$ sum (*32*). Backbone dihedral angles ϕ and ψ were predicted from ^{15}N, $^{13}C_\alpha$, $^{13}C_\beta$, ^{13}CO, and $^1H_\alpha$ chemical shifts using TALOS (*33*). Dihedral angles were restrained to ±30° and ±50° for α-helices and β-strands, respectively. Hydrogen bond restraints were obtained from hydrogen−deuterium exchange experiments. Uniformly ^{15}N-labeled SopE2$_{69-240}$ in NMR buffer was lyophilized and resuspended in 99.96% D_2O. A series of ^{1}H−^{15}N HSQC spectra was then recorded to identify the amide protons protected from exchange with the solvent. NH resonances remaining after 2 h were assigned as having hydrogen bonds. For hydrogen bond distance constraints, the NH−O distance was set between lower and upper distance bounds of 1.5 and 2.8 Å and the N−O distances to lower and upper distance bounds of 2.4 and 3.5 Å, respectively.

Structures were calculated using XPLOR-NIH version 2.06 (*34*), using the standard simulated annealing protocol starting from random extended structures. Default values were used for all force constants and molecular parameters. The ensemble of NMR structures was analyzed for violated restraints using the VMD-XPLOR visualization package (*35*). The structure calculation was carried out iteratively whereby consistently violated restraints were reassigned, wherever possible, using existing structures or removed until a consistent set of constraints was obtained with few violations in the ensemble. The ensemble of structures was further refined with XPLOR-NIH standard refinement protocols using the final set of restraints. The quality of the structures was checked using PROCHECK-NMR (*36*). Structure figures were generated with MOLMOL 2K.1 (*37*).

Backbone ^{15}N Relaxation Measurement and Analysis. Relaxation experiments were performed at 25 °C on 1.0 mM ^{15}N-labeled SopE2$_{69-240}$. R_1 spectra (*38*) were acquired with 512 (t_2) × 256 (t_1) complex points with spectral widths of 8000 Hz in ^{1}H and 2000 Hz in ^{15}N and 24 scans per t_1 point. A recycle delay of 1.8 s was employed. Relaxation delay times of 10 (2), 40 (3), 100 (3), 240 (2), 400 (2), 600 (2), 850 (2), and 1100 ms (2) were used, where the number in parentheses indicates the number of times each experiment was performed.

$R_{1\rho}$ spectra (*39*) were acquired with 512 complex ^{1}H points and 192 complex ^{15}N points with 32 scans per increment and spectral widths of 8000 Hz in ^{1}H and 2000 Hz in ^{15}N. The recycle delay was 3.0 s, and a ^{15}N spin lock field of 1.5 kHz was employed. Relaxation delays of 8, 20, 32, 44, 58, 77, 86, and 100 ms were used, with two data sets acquired for each delay. Steady-state [^{1}H]−^{15}N NOEs were determined from spectra recorded with (NOE experiment) and without (NONOE experiment) a proton presaturation period of 5 s. A recycle delay of 12 s was employed in the NONOE experiments, whereas a recycle delay of 7 s was used prior to the 5 s presaturation period in the NOE experiments (*38*). NOE and NONOE spectra were acquired alternately to reduce time-dependent artifacts with 512 complex ^{1}H points and 192 complex ^{15}N points with 32 scans per increment. NOE and NONOE experiments were each carried out three times.

The relaxation spectra were processed with the NMRPipe/NMRDraw suite (*27*) and analyzed with SPARKY (*28*). The R_1 and $R_{1\rho}$ relaxation rates were obtained by fitting relative peak heights as a function of the R_1 and $R_{1\rho}$ delay time to a two-parameter exponential in Curvefit (A. G. Palmer, III, Columbia University, New York, NY). Errors in R_1 and $R_{1\rho}$ were calculated using Curvefit. ^{15}N T_2 values were obtained from measured $R_{1\rho}$ and R_1 rates as described by Korzhnev *et al.* (*39*). The value of the steady-state NOE was calculated as the average ratio of peak intensities in the presence and absence of proton saturation. The uncertainties in the steady-state NOE values are reported as the standard deviation of the NOE measurements.

The overall rotation of the molecule was analyzed to separate its contributions to relaxation from those of site-specific internal motions. An initial estimate of the global correlation time (τ_c) was determined from the R_2/R_1 values (*40*) using the r2r1_tm software (A. G. Palmer, III). Residues with low NOE values (<0.65) and residues with above-average R_2 values not having correspondingly low R_1 values were eliminated from the analysis due to possible fast internal motions. Estimates of the components of the molecular rotational diffusion tensor were made using the atomic coordinates of the NMR solution structure of SopE2$_{69-240}$ closest to the mean. PDB_Inertia version 1.1 (A. G. Palmer, III) was used to transform the coordinates so that the center of mass was at the origin, and the principal axes of the point-

mass rotational inertia tensor were aligned with the coordinate axes. Estimates of axial and fully anisotropic diffusion tensors were obtained by applying minimization techniques using Quadric_Diffusion 1.11 (*41*). On the basis of *F* statistic testing, the rotational diffusion tensor was assumed to be axially symmetric (*41*).

The relaxation data were analyzed according to the extended Lipari−Szabo model-free formalism (*42*, *43*) implemented in TENSOR2 (*44*). Model selection was based on 500 Monte Carlo simulations using a simulated annealing algorithm to characterize the random variation in the fit and to provide probability statistics and error analysis. Data were fit to five standard models [S^2 (model 1), S^2 and τ_e (model 2), S^2 and R_{ex} (model 3), S^2, τ_e, and R_{ex} (model 4), and S^2, S_f^2, and τ_e (model 5)] selected on the basis of *F* statistics (*38*).

Chemical Shift Mapping of the SopE2$_{69-240}$−Cdc42 Complex. Binding of unlabeled Cdc42Δ7 to ^{15}N-labeled SopE2$_{69-240}$ was followed by chemical shift perturbation in ^{1}H−^{15}N HSQC spectra. Cdc42Δ7 was purified from *Escharichia coli* BL21(DE3) as previously described (*19*). The titration was performed as previously described (*45*). Briefly, two initial NMR samples were prepared in 0.5 mL of NMR buffer with 10% D_2O. Sample A contained 0.5 mM SopE2$_{69-240}$ (SopE2$_{69-240}$:Cdc42Δ7 molar ratio of 1:0), and sample B contained 0.5 mM SopE2$_{69-240}$ and 1.34 mM Cdc42Δ7 (SopE2$_{69-240}$:Cdc42Δ7 molar ratio of 1:2.67). The buffer composition of both samples was identical as both samples were extensively exchanged into the same batch of sample buffer. Throughout the titration, the concentration of SopE2$_{69-240}$ was maintained at a constant concentration of 0.5 mM and the Cdc42Δ7 concentration was varied to give a series of SopE2$_{69-240}$:Cdc42Δ7 molar ratios from 1:0 to 1:2.67. A ^{1}H−^{15}N HSQC spectrum was acquired at each titration point with 512 complex ^{1}H points and 192 complex ^{15}N points with 40 scans per increment and spectral widths of 8000 Hz in ^{1}H and 2000 Hz in ^{15}N. The initial NMR samples represented the end points of the titration. Intermediate values of the SopE2$_{69-240}$:Cdc42Δ7 ratio were obtained by simultaneously taking equal aliquots from both sample A and sample B and then transferring the aliquots to the other NMR tube (i.e., from tube A to tube B and vice versa). This procedure was repeated until a series of 12 ^{1}H−^{15}N HSQC experiments at SopE2:Cdc42Δ7 molar ratios of 1:0, 1:0.05, 1:0.11, 1:0.22, 1:0.47, 1:0.56, 1:0.77, 1:1.1, 1:1.21, 1:1.47, 1:1.80, and 1:2.67 had been completed.

RESULTS

Structure of the SopE2 Catalytic Domain. The structure of SopE2$_{69-240}$ was determined using 2548 distance restraints (comprising 883 intraresidue, 1218 sequential and medium-range, and 447 long-range NOEs), 134 hydrogen bond restraints, and 249 ψ and ϕ dihedral restraints. A total of 20 structures was chosen to represent the ensemble of NMR structures on the basis of lowest-energy and minimal distance and torsional angle restraint violations. All of these structures were consistent with both experimental data and standard covalent geometry, displaying no violations greater than 0.5 Å for distance restraints or 5° for dihedral angles. Details of the final set of structural restraints and their violations within the final ensemble are listed in Table 1. The ensemble of structures and the structure closest to the mean are shown in Figure 2. The ensemble of structures has a backbone and all heavy atom rmsds from the mean over the regular secondary structure elements of 0.75 and 1.60 Å, respectively. A Ramachandran plot of the structures with PROCHECK-NMR (*36*) indicates that 96.5% of the residues (excluding Gly and Pro residues) lie in the most favored or additionally allowed regions. The few non-glycine residues to fall into the generously allowed regions and disallowed regions correspond to residues located at the termini or loop regions where the NMR restraint density is low. A single structure closest to the mean of the ensemble was chosen for illustrative purposes and for further discussion.

Table 1: Structural Statistics on the Final Set of NMR-Derived Structures of the SopE2 GEF Domain

no. of total NOE restraints	2548
intraresidue	883
sequential/medium-range (residue *i* to *i* + 1−5)	1218
long-range	447
no. of dihedral angle restraints	
backbone ψ and ϕ	249
hydrogen bond	134
rmsd for backbone atoms	0.75,[a] 0.67[b]
rmsd for heavy atoms	1.60,[a] 1.60[b]
average no. of NOE violations	
>0.3 Å (per structure)	11
>0.5 Å (per structure)	0

	representative structure	ensemble
Ramachandran plot regions[c]		
most favored (%)	86.2	84.6
additional allowed (%)	11.7	11.9
generously allowed (%)	1.4	2.1
rmsd from ideal geometry		
bonds (Å)	0.00788271	0.0077672
angles (deg)	0.9335	0.9381
improper (deg)	0.8125	0.8283

[a] The rmsd from the mean structure calculated over residues 80−132, 138−150, 154−164, 173−183, 191−208, and 222−236. [b] The rmsd from the mean structure calculated over residues 80−132, 138−150, 173−183, 191−208, and 222−236. [c] Calculated with PROCHECK-NMR (*36*).

SopE2$_{69-240}$ consists of six α-helices arranged in two three-helix bundles, α1α4α5 and α2α3α6. The two bundles are arranged in a Λ shape (Figure 2B) with the relative orientation of the bundles defined by 20 interbundle NOEs. The three-helix bundles are connected by a turn between helices α1 and α2, a β-hairpin (residues 154−164) followed by a loop that contains the ^{166}GAGA^{169} catalytic motif between helices α3 and α4, and a loop between helices α5 and α6. The β-hairpin displays an rmsd that is higher than those of other secondary structure elements, and omission of the β-hairpin from the calculation lowers the backbone rmsd from 0.75 to 0.67 Å.

Comparison of the SopE2$_{69-240}$ NMR Structure with the SopE$_{78-240}$ Crystal Structure. The secondary structure and global fold of the *S.* Dublin SopE2$_{69-240}$ NMR solution structure are similar to those reported for the Cdc42-bound *S.* Typhimurium SopE catalytic domain (*24*). There are differences in the lengths of some of the regular secondary structure elements between SopE2$_{69-240}$ and Cdc42-bound SopE$_{78-240}$. In particular, helix α1 spans residues 81−93 in the SopE$_{78-240}$ structure, but in SopE2$_{69-240}$, this helix spans

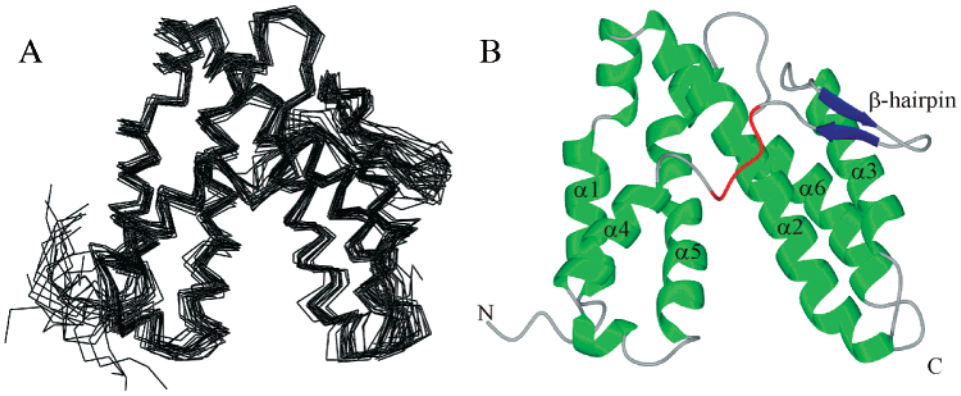

FIGURE 2: Structure of the SopE2 GEF domain (residues 69−240). (A) Backbone (N, C^{α}, and C′) trace of the 20 lowest-energy structures. (B) Ribbon diagram of the structure closest to the mean. The α-helices and *β*-hairpin are labeled. The ^{166}GAGA^{169} catalytic motif is highlighted in red. The figure was generated with MOLMOL (*37*).

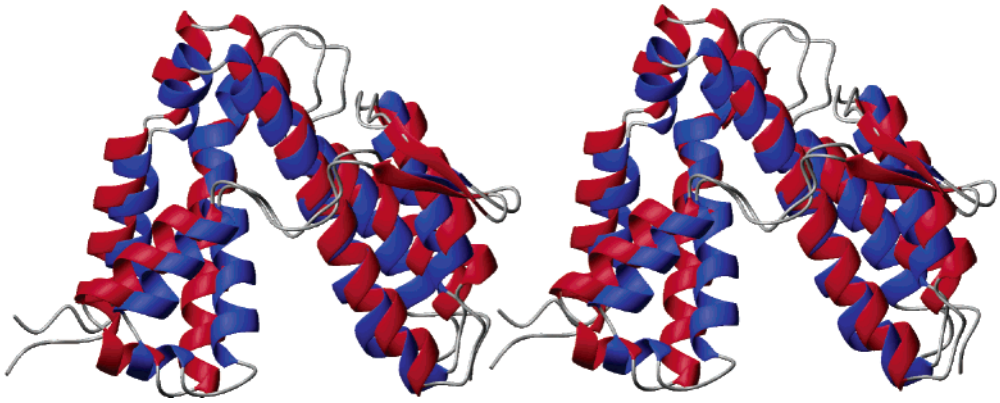

FIGURE 3: Backbone superposition (residues 83−236) shown in stereo of the solution structure of $SopE2_{69-240}$ (blue) with the crystal structure of Cdc42-bound $SopE_{78-240}$ (red; PDB entry 1GZS) (*24*), demonstrating the similarities and differences in the two structures. The structures superimposed with a backbone rmsd of 2.26 Å. Both structures consist of two three-helix bundles with one linker comprising a *β*-hairpin followed by a loop that contains the ^{166}GAGA^{169} catalytic motif.

residues 83−93. An overlay of the representative $SopE2_{69-240}$ NMR structure with the 2.3 Å resolution Cdc42-bound $SopE_{78-240}$ crystal structure is shown in Figure 3; the structures superimpose with a backbone rmsd of 2.26 Å over the structurally ordered portions (residues 83−236). Superimposing the three-helix bundles individually results in a lower rmsd between $SopE2_{69-240}$ and $SopE_{78-240}$: helices α1, α4, and α5 have an rmsd of 1.29 Å, and helices α2, α3, and α6 have an rmsd of 1.48 Å. Conformational differences between unbound $SopE2_{69-240}$ and Cdc42-bound $SopE_{78-240}$ can be further quantified by comparison of the interhelix angles (Table 2). The binding of Cdc42 to $SopE_{78-240}$ results in an opening of the structure leading to a change in the crossing angles of several pairs of helices of 10−11° relative to those observed in unbound $SopE2_{69-240}$ in solution. Cdc42-bound $SopE_{78-240}$ is consequently less compact than unbound $SopE2_{69-240}$. Although $SopE_{78-240}$ helices α2 and α5 show a relatively small change in overall orientation upon binding, the lower halves of these helices start to diverge from the unbound $SopE2_{69-240}$ structure around residue 122 in α2 and residue 206 in α5, resulting in a splaying of the helices.

Backbone ^{15}N Dynamics of $SopE2_{69-240}$. To assess the potential contributions of dynamics to SopE2 function, we measured the backbone ^{15}N T_1 and T_2 and [^{1}H]−^{15}N NOE values of $SopE2_{69-240}$ (Figure 4). Of the 149 assigned residues in $SopE2_{69-240}$, relaxation data were obtained for 140 residues. Data could not be fitted satisfactorily for nine residues due to overlap (Arg75, Ala167, Ile177, Ala201, Lys203, Lys207, Thr210, and Thr225) or because cross-peaks were absent (Leu78). These measurements (Figure 4) indicate that the helical segments have a relatively uniform relaxation rate whereas the termini and loop regions, in particular the ^{166}GAGA^{169} catalytic loop and the loop connecting helices α5 and α6 (residues Asn214−Thr220), are more flexible.

Table 2: Comparison of Helix Crossing Angles in the Three-Helix Bundles of the Crystal Structure of Cdc42-Bound $SopE_{78-240}$ and the Solution Structure of $SopE2_{69-240}$

	crossing angle (deg)[a]		
helix pair	SopE[b]	SopE2	Δ (SopE2 − SopE)[c]
1−2	−141.08	−149.36	−8.28
1−3	−43.49	−32.32	11.17
1−4	132.28	131.71	−0.56
1−5	−35.21	−31.76	3.45
1−6	123.33	134.07	10.74
2−3	165.24	161.34	−3.89
2−4	−79.58	−76.45	3.13
2−5	−133.28	−134.40	−1.12
2−6	−17.78	−19.65	−1.87
3−4	105.35	112.53	7.18
3−5	38.08	31.15	−6.93
3−6	159.99	163.25	3.26
4−5	142.39	141.83	−0.55
4−6	−94.23	−84.18	10.05
5−6	121.91	132.82	10.91

[a] Calculated with Interhlx (K. Yap, University of Toronto). [b] SopE GEF domain from the crystal structure (PDB entry 1GZS). [c] The $SopE2_{69-240}$ helix crossing angle minus the $SopE_{78-240}$ helix crossing angle.

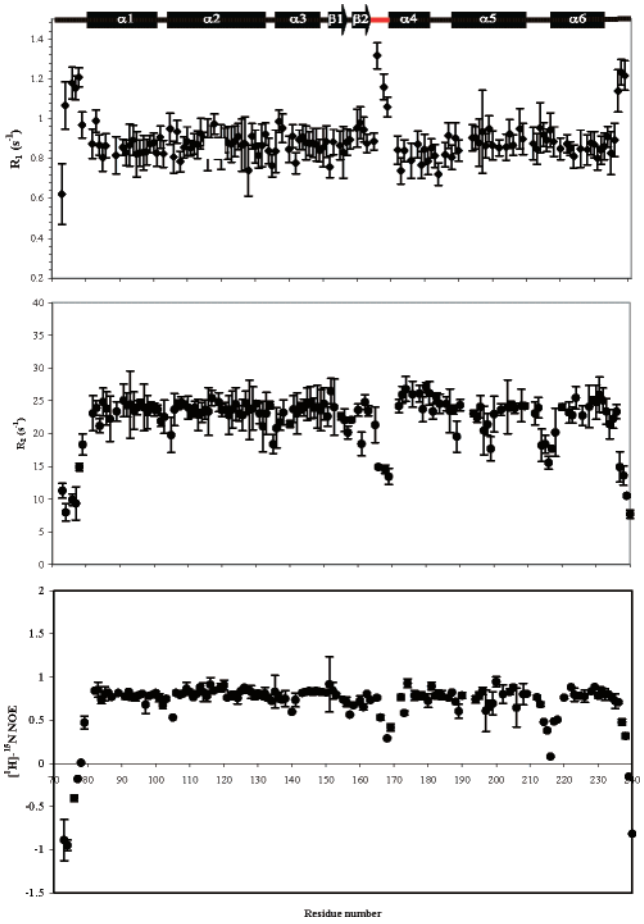

FIGURE 4: Plots as a function of residue number of backbone ^{15}N R_1 and R_2 and [^{1}H]−^{15}N NOE for uniformly ^{15}N-labeled SopE2$_{69-240}$ at pH 7.0, 14.1 T (600 MHz), and 25 °C. Error bars represent experimental errors in measurement. Secondary structure elements are represented at the top of the figure as arrows (β-strands) and rectangles (α-helices); the loop containing the ^{166}GAGA^{169} catalytic motif is highlighted in red.

The termini and loop regions also exhibited below-average [^{1}H]−^{15}N NOE values, indicating contributions to their relaxation from internal dynamics on the sub-nanosecond time scale. In addition to these loop regions, there are also residues with below-average R_2 values in regions of regular secondary structure (Ala105 in α2, β-hairpin residues 157−164, and Phe197 and Ala199 in α5), indicating that the relaxation of these amide ^{15}N nuclei is dominated by overall tumbling of the molecule.

Using the NMR solution structure of SopE2$_{69-240}$ closest to the mean, the R_2/R_1 relaxation data could be fit in terms of an axially symmetric diffusion tensor with a $D_{||}/D_{\perp}$ ratio of 0.884. A fit of the R_2/R_1 values yielded an overall correlation time, τ_c, of 16.65 ± 0.40 ns. This value of τ_c is larger than expected for an 18.2 kDa protein based on previously studied proteins or from the Stokes−Einstein relation which predicts a value of 8 ns when a 3.0 Å water layer is included. The oblate shape of SopE2$_{69-240}$, combined with an elongated N-terminus (residues 69−80) that extends into the solvent, may account at least partially for this relatively high τ_c value. Indeed, hydrodynamic calculations based on the SopE2$_{69-240}$ atomic coordinates using HYDRONMR (*46*) give an overall correlation time of 13.2 ns. The discrepancy between this value and 16.65 ± 0.40 ns may derive from reversible association of SopE2$_{69-240}$ monomers into dimers and/or larger multimers. This possibility is discussed further below.

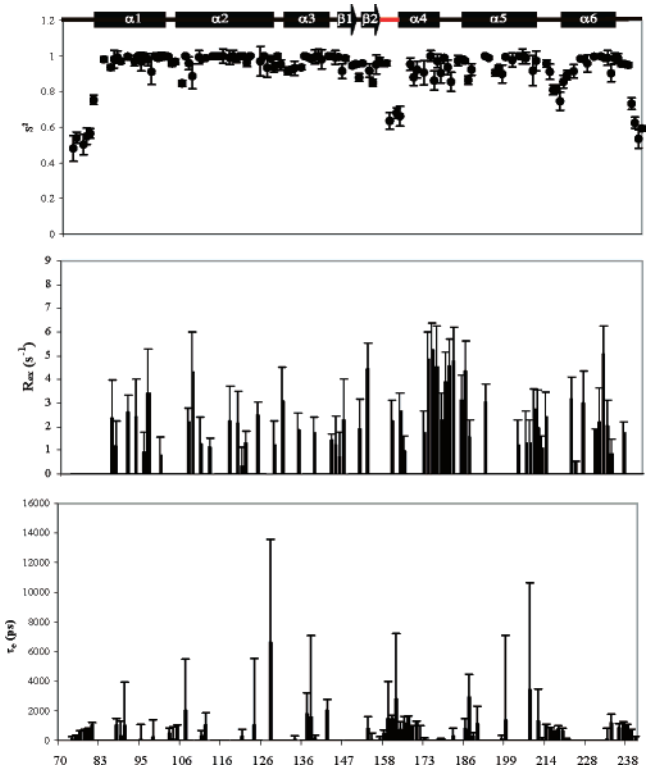

FIGURE 5: Plots as a function of residue number of the order parameter, S^2 (top panel), the effective correlation time, τ_e (bottom panel), and the chemical exchange term, R_{ex} (middle panel), for uniformly ^{15}N-labeled SopE2$_{69-240}$ at pH 7.0, 14.1 T (600 MHz), and 25 °C. Secondary structure elements are represented at the top of the figure as arrows (β-strands) and rectangles (α-helices); the loop containing the ^{166}GAGA^{169} catalytic motif is highlighted in red.

Model-free analysis of the NMR relaxation data was performed using the program TENSOR2 (*44*). Model selection was performed using the *F* test strategy of Mandel *et al.* (*47*). The relaxation parameters could be fit within experimental error for all but six residues, indicating that the model cannot account for the additional contributions to the relaxation of these six residues. The generalized order parameter (S^2), the effective correlation time (τ_e), and the chemical exchange term (R_{ex}) are plotted as a function of residue in Figure 5, and the solution structure of SopE2$_{69-240}$ is shown color-coded according to S^2 values in Figure 6. An average S^2 value of 0.92 ± 0.03 was obtained. Typically, the S^2 values for the regular secondary structure elements fall into the range of 0.9−1.0, indicative of highly restricted backbone motions on the sub-nanosecond time scale. Residues with the lowest S^2 values or S_f^2 values are located at or near the N- and C-termini and in loops, with below-average S^2 values also exhibited by residues located in the β-hairpin and in helices α2, α4, and α5. It is also notable that there are clusters of qualitatively large τ_e values in the β-hairpin, in the catalytic loop, and in the loop between helices α5 and α6.

Numerous residues require an exchange term, R_{ex} (Figure 5). To avoid artifacts caused by model selection, the detected R_{ex} values were checked for compatibility with the original relaxation data. The largest cluster of residues requiring R_{ex} is located at helix α4, where the R_{ex} terms probably do not

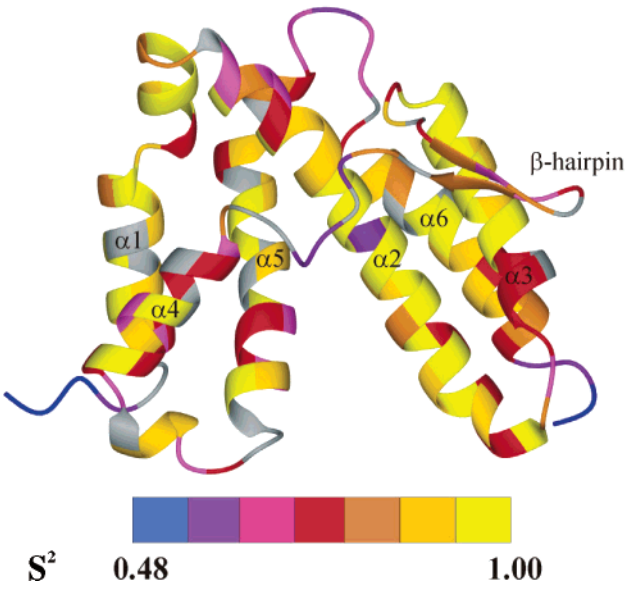

FIGURE 6: Solution structure of SopE2$_{69-240}$ color-coded by the generalized order parameter, S^2. The S^2 color scheme is interpolated continuously from 0.48 (purple) to 1.0 (yellow). Residues for which no order parameter was obtained are colored gray.

reflect chemical exchange but arise from the unique orientation of this helix relative to the other helices in SopE2$_{69-240}$ (Figures 2 and 3). Consequently, helix α4 experiences a longer rotational correlation time than the other helices, as demonstrated by a smaller R_1 and a larger R_2 for residues in helix α4 relative to those in other helices. Nevertheless, α4 does not align well with the long axis of the rotational diffusion tensor and is tilted from it by an angle of ca. 55°. The R_{ex} terms for residues in helices α1−α3 are unlikely to be due to molecular anisotropy since these terms do not occur throughout the helices, but rather are confined to residues located on the solvent-exposed faces of these α-helices. This suggests that there is an exchange event that affects the protein surface. One possibility is oligomerization, which would be consistent with the relatively large τ_c of SopE2$_{69-240}$; the R_{ex} terms in helices α1−α3 could then be a consequence of exchange due to interaction with other SopE2$_{69-240}$ molecules. ^{1}H−^{15}N HSQC spectra measured at protein concentrations over the range of 0.5−1.5 mM did not indicate any evidence of oligomerization, however, suggesting that oligomerization is weak if it occurs at all. Interestingly, there are clusters of residues exhibiting R_{ex} terms in and between helices α5 and α6. The original relaxation data for residues at the C-terminus of α5 and the beginning of the loop support the presence of R_{ex} terms, exhibiting average R_2 and below-average [^{1}H]−^{15}N NOE values. This relaxation profile is typical of residues undergoing both microsecond and millisecond motion.

Mapping the Binding Site of Cdc42 onto the Solution Structure of SopE2$_{69-240}$. To follow the effect of SopE2$_{69-240}$ binding to Cdc42 in solution, 12 2D ^{1}H−^{15}N HQSC experiments with various mixtures of uniformly ^{15}N-labeled SopE2$_{69-240}$ and unlabeled human Cdc42Δ7 were performed. Changes in SopE2$_{69-240}$ ^{1}HN and ^{15}N chemical shifts between the free state and the Cdc42Δ7-complexed state were calculated using the formula $\Delta\delta_{ave} = [\Delta\delta_{HN}^2 + (\Delta\delta_N^2/25)/2)]^{1/2}$, where $\Delta\delta_{HN}$ and $\Delta\delta_N$ correspond to the chemical shift difference in the amide proton and ^{15}N chemical shifts between the free and complexed state, respectively. This analysis revealed that numerous resonances are significantly perturbed upon binding to Cdc42Δ7. When mapped onto the solution structure of SopE2$_{69-240}$, the residues displaying the greatest chemical shift changes fall into two groups. The first group of residues is located on the face of SopE2$_{69-240}$ that corresponds to the SopE binding interface (Figure 7A) and includes residues from helices α2 and α4−α6 and the ^{166}GAGA^{169} catalytic loop. In addition to changes in backbone NH resonances, this group includes chemical shift changes for the side chain NH_2 resonances of Q109 (helix α2) and Q194 (helix α5). This group of residues shows very good agreement with the SopE$_{78-240}$ residues involved in important intermolecular interactions in the SopE$_{78-240}$−Cdc42 crystal structure (Figure 7B), where the complex interface was primarily formed by SopE$_{78-240}$ helices α2, α4, and α5 and the catalytic loop (*24*). The second group of

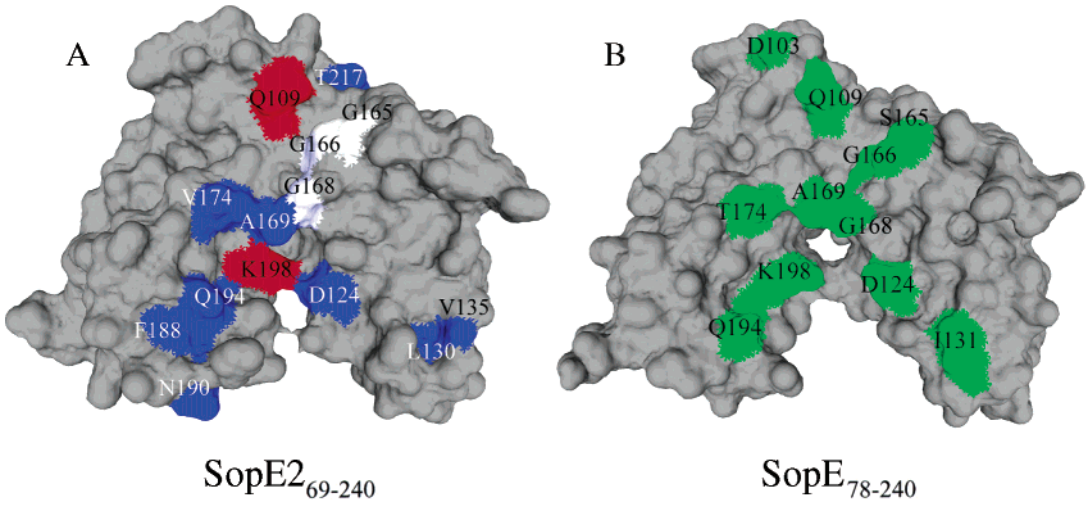

FIGURE 7: Comparison of SopE2$_{69-240}$ and SopE$_{78-240}$ interaction surfaces. (A) Chemical shift perturbations in SopE2$_{69-240}$ caused by binding to Cdc42Δ7 are mapped onto a molecular surface representation of the energy-minimized structure of SopE2$_{69-240}$ closest to the mean. Residues with shift perturbations ($\Delta\delta_{ave}$) of ≥10 Hz are colored red and those with a $\Delta\delta_{ave}$ between 5 and 10 Hz blue. Gray indicates little or no change in chemical shift upon binding. Residues highlighted in white experience severe line broadening due to interaction with Cdc42. (B) Molecular surface representation of SopE$_{78-240}$ taken from the SopE$_{78-240}$−Cdc42 complex crystal structure (*24*). SopE$_{78-240}$ residues highlighted in green are those involved in important interactions with Cdc42 in the SopE$_{78-240}$−Cdc42 complex crystal structure.

perturbed $SopE2_{69-240}$ residues comprises several scattered internal residues and isolated residues on the side of the molecule opposite from the binding interface. Such scattered effects observed outside the binding regions are probably caused by indirect effects of interaction of $SopE2_{69-240}$ with Cdc42.

DISCUSSION

SopE2 and its close homologue SopE play a pivotal role in *Salmonella* invasion of host cells by functioning as GEFs for Rho GTPases Cdc42 and Rac1. The 2.3 Å crystal structure of $SopE_{78-240}$ in complex with Cdc42 (*24*) established the overall architecture of the SopE−Cdc42 complex and revealed that the binding of $SopE_{78-240}$ to Cdc42 induces conformational rearrangements in the Cdc42 nucleotide binding site that are strikingly similar to those observed in DH GEF−Rho GTPase complexes (*11*−*13*). Inspection of the binding interface revealed that a number of $SopE_{78-240}$ residues involved in stabilizing the rearranged nucleotide binding region form polar contacts with Cdc42 residues, in a fashion analogous to that of residues in the DH GEFs. The studies reported here, including comparison of the $SopE2_{69-240}$ solution structure to the Cdc42-bound $SopE_{78-240}$ crystal structure, dynamics, and interaction studies, provide the first details of the changes in SopE/E2 structure that occur upon Cdc42 binding. The dynamics studies reveal that residues linking the two three-helix bundles of SopE2, including the catalytic loop, are flexible on a range of time scales. We propose that this flexibility plays an important role in target protein binding and catalysis.

Solution Structure of $SopE2_{69-240}$ and Comparison to Cdc42-Bound $SopE_{78-240}$. Comparison of the NMR structure of unbound $SopE2_{69-240}$ in solution to the crystal structure of Cdc42-bound $SopE_{78-240}$ reveals that the two structures have similar global folds (Figure 3). Free $SopE2_{69-240}$, however, has a more closed Λ than Cdc42-bound $SopE_{78-240}$ due to movement of helices α2 and α5 to accommodate binding of Cdc42 switch I and II regions. Secondary effects due to Cdc42 binding lead to a change in the orientation of helices α1, α3, and α6. The unbound SopE2 GEF domain is consequently more compact than the Cdc42-bound SopE GEF domain, and these global conformational changes are largely responsible for an rmsd for the backbone atoms of residues 83−236 between free $SopE2_{69-240}$ and Cdc42-bound $SopE_{78-240}$ of 2.26 Å.

The greatest conformational changes to occur in the binding site are in the lower halves of helices α2 and α5. In $SopE2_{69-240}$, these helices start to diverge from those in Cdc42-bound $SopE_{78-240}$ at Asn122 in helix α2 and Met206 in helix α5, leading to an overall displacement at the N-terminus of helix α2 and at the C-terminus of helix α5 of ∼2.5 Å when compared to Cdc42-bound $SopE_{78-240}$. In Cdc42-bound $SopE_{78-240}$, residues in the lower half of helices α2 and α5 are primarily involved in stabilizing the displaced switch I region of Cdc42 following insertion of the SopE ^{166}GAGA^{169} catalytic loop. When compared with the GDP-bound Cdc42 structure, the interaction of $SopE_{78-240}$ with Cdc42 displaces the switch I region by up to 2.7 Å. This suggests that structural plasticity of helices α2 and α5 may be critical for catalysis.

$SopE2_{69-240}$−Cdc42 Titration. The interaction between $SopE2_{69-240}$ and Cdc42 was monitored using ^{1}H−^{15}N NMR spectroscopy. On the basis of chemical shift changes observed in ^{1}H−^{15}N HSQC spectra of $SopE2_{69-240}$, numerous $SopE2_{69-240}$ backbone NH and side chain NH_2 groups were perturbed upon binding Cdc42. There is excellent agreement between those $SopE2_{69-240}$ residues most strongly perturbed by binding Cdc42 and $SopE_{78-240}$ residues involved in key interactions at the molecular interface in the $SopE_{78-240}$−Cdc42 complex crystal structure. These residues are mapped onto the respective $SopE2_{69-240}$ and $SopE_{78-240}$ molecular surfaces for comparison in Figure 7. The list includes Gln109 (α2), Asp124 (α2), Val/Thr174 (catalytic loop), Gln194 (α5), and Lys198 (α5), which are involved in making polar contacts with Cdc42 residues to stabilize the rearranged switch regions in the $SopE_{78-240}$−Cdc42 complex (*21*, *24*), and Gln109 (α2), Asp124 (α2), and Gly168 (catalytic loop), which have been shown by mutagenesis to be critical for nucleotide release (*21*). Resonances due to several other residues in the ^{166}GAGA^{169} catalytic loop of $SopE2_{69-240}$ were also strongly perturbed upon binding, for example, $Ala169_{SopE2}$; in the $SopE_{78-240}$−Cdc42 complex, $Ala169_{SopE}$ stabilizes the reorientation of $Ala59_{Cdc42}$ through main chain interactions and results in the Mg^{2+} binding site being blocked. The peaks due to G165, G166, and G168 in the catalytic loop were severely broadened and were beyond detection before the $SopE2_{69-240}$:Cdc42 ratio reached 1:0.75, supporting the close location of these residues to the intermolecular surface between Cdc42 and SopE2. It is intriguing that, in addition to helix α5 residues, the chemical shifts of several residues in helix α6 were perturbed upon binding Cdc42, including a $\Delta\delta_{ave}$ of 16 Hz for the backbone NH of Gln223. This may reflect a change in the relative orientation of α5 and α6 as the three-helix bundles move apart upon binding Cdc42. Several scattered internal residues and residues present on the side of the molecule opposite from the binding interface were also perturbed upon binding to Cdc42; it is important to note that chemical shifts are very sensitive to changes in the local environment, and these perturbations probably arise from induced indirect conformational changes.

With respect to the question of SopE/E2 specificity for Rho GTPases [*S.* Typhimurium $SopE_{78-240}$ is an equally efficient GEF for both Rac1 and Cdc42, whereas *S.* Typhimurium $SopE2_{69-240}$ is a more efficient GEF for Cdc42 than SopE, but is a less active GEF for Rac1 (*20*)], it is worth noting that if SopE and SopE2 mimic the DH GEF mechanism of nucleotide release, they may also utilize the so-called "specificity patch" of Rho GTPases, located between the switch regions (*11*, *13*), to dictate substrate specificity. In support of this idea, the regions of SopE and SopE2 that bind to the Rho GTPase specificity patch (SopE/E2 residues 174−194) show considerable sequence divergence between SopE and SopE2 (Figure 1). In *S.* Dublin, for example, a number of polar SopE residues (Thr174, Thr178, and Ser182) involved in binding to the Rho GTPase specificity patch are nonconservatively replaced with hydrophobic residues (Val174, Ala178, and Ile182) in SopE2.

Backbone Dynamics of $SopE2_{69-240}$. Protein function is closely related not only to three-dimensional structure but also to molecular motion. Dynamics plays an important part in Rho GTPase interactions: the switch regions of the Rho GTPases are highly dynamic, undergoing extensive motion on a variety of time scales in both the inactive GDP and active GTP states (*48*−*51*). Numerous different proteins,

including GEFs, GTPase activating proteins, guanine nucleotide dissociation inhibitors, and several protein kinases, interact directly with the switch regions, and the flexibility of these regions is a critical factor in Rho GTPase function.

NMR relaxation studies can provide detailed, residue-specific information about protein dynamics and consequently can be used in combination with structural data to gain a deeper understanding of protein function (*52*). To shed light on the role of dynamics in Rho GTPase interactions with the SopE-like GEFs, we have measured backbone ^{15}N relaxation parameters for $SopE2_{69-240}$. These measurements show that the secondary structure of $SopE2_{69-240}$ is generally rigid with an average S^2 value of 0.92 ± 0.03 (Figures 5 and 6). Interestingly, the β-hairpin residues (154−164) close to the ^{166}GAGA^{169} catalytic region have an average [^{1}H]−^{15}N NOE of 0.68 ± 0.02, lower than the average [^{1}H]−^{15}N NOE of 0.79 ± 0.05 over all of the α-helices, and require qualitatively large effective correlation times, τ_e (Figure 5), suggesting that there is flexibility in the β-hairpin. On the basis of the combination of structural data (restraints that result in the β-hairpin in the calculated structures) and dynamics data, one might speculate that the β-hairpin undergoes fractional melting or cooperative motion. As expected, the loop regions, in particular, the catalytic loop between the β-hairpin and helix α4 and much of the loop connecting helices α5 and α6, exhibit mobility on a variety of time scales from sub-nanoseconds to milliseconds, as judged by the low values of [^{1}H]−^{15}N NOE (Figure 4) and S^2 (Figure 5) and the requirements for qualitatively large effective correlation times, τ_e, and a two-time scale spectral density model. Apart from helix α4, moreover, the C-terminus of helix α5, part of the α5−α6 loop, and helix α6 constitute the most significant cluster of residues requiring R_{ex} terms (Figure 5). The R_{ex} terms in helix α4 probably arise from its unique orientation within the protein, whereas the α5−α6 R_{ex} terms are more likely to reflect exchange between multiple conformations, as also indicated by the values of R_1, R_2, and [^{1}H]−^{15}N NOE in the α5−α6 loop. The mobility indicated by the ^{15}N relaxation parameters in the β-hairpin, catalytic loop, and α5−α6 loop that together link the two three-helix bundles (Figure 2) is in accord with the significant lowering of the rmsd among the ensemble of structures when individual three-helix bundles are compared relative to when all secondary structure elements are included. The dynamics and structural data both indicate that the relative orientation of the helical bundles in $SopE2_{69-240}$ is flexible.

In addition to the β-hairpin and catalytic loop, there are a number of mobile "hot spots" involving $SopE2_{69-240}$ residues that correspond to SopE residues involved in engaging and stabilizing Cdc42 in the SopE−Cdc42 complex (Figures 1 and 4−6). These include the N- and C-termini of helix α2 and helix α5. As described above, both of these helices undergo significant conformational change when compared to the structure of Cdc42-bound $SopE_{78-240}$, and both are involved in pushing the switch I region of Cdc42 aside and subsequently stabilizing the altered conformation in the SopE−Cdc42 complex.

An induced fit model has been proposed for DH GEF-mediated nucleotide release (*11*). The apparent mechanistic similarity between eukaryotic DH GEFs and SopE (*24*) leads to a proposal for SopE/E2 GEF action in which SopE/E2 first interacts with the conformationally rigid portions of the GTPase to provide sufficient binding energy for catalysis. Following this initial "lock and key" interaction, an "induced fit" results in the altered conformation of the switch I−II regions. The general rigidity of the individual three-helix bundles would allow initial binding of SopE2 to its target protein with sufficient affinity and specificity. The flexibility in the relative three-helix bundle orientation, including the catalytic loop, and local mobility in helices α2 and α5 indicated by our NMR studies could then permit adjustments in conformation for maximization of favorable contacts at the interface and accommodation of alterations in the switch regions of the GTPase that promote nucleotide release. The previously measured association rate constants for interaction of SopE/E2 with Cdc42 and Rac1, all on the order of 10^5 M^{-1} s^{-1} (*19*, *20*), show that the association is not in the diffusion limit. This suggests that SopE/E2−GTPase association is controlled by a rare event, compatible with the notion that fast, diffusion-controlled collision of GEF and GTPase is followed by much slower structural change(s), resulting in the final bound conformation of the complex.

The flexibility of the SopE2 catalytic loop on both sub-nanosecond and microsecond to millisecond time scales, including the catalytic ^{166}GAGA^{169} residues, is likely to be important for its catalytic role: the observed flexibility would seem to be necessary for ^{166}GAGA^{169} to induce conformational changes in the Rho GTPase switch regions to ones more favorable for nucleotide release. As mentioned above, the switch regions are highly dynamic even when bound to an effector (*50*, *51*). It has been suggested that flexibility of the GTPase switch regions is not only important for tight, high-affinity binding of the GTPase to its partner but also critical for efficient GDP−GTP exchange. As such, the flexibility of the ^{166}GAGA^{169} loop of SopE/E2 would not only help to induce conformational changes in the switch regions sufficient to destabilize nucleotide binding but also may inhibit freezing of the switch regions into a single conformation that would prevent the release of bound GDP.

Flexibility of the kind demonstrated here for SopE2 may enable SopE/E2 to bind to and stimulate nucleotide release for substrates in addition to Cdc42 and Rac1 through adaptive binding: previous reports have shown that the SopE-like GEFs can act on a variety of GTPases (*20*, *25*). There is evidence (*53*), moreover, that SopE2 is able to bind non-GTPase proteins such as the calcium binding protein allograft inflammatory factor 1 (AIF1), which probably participates in the regulation of actin, and cholesterol binding protein apolipoprotein A-1 (Apo-A1). The presence of individually conformationally rigid three-helix bundles with flexibility in their relative orientation may be important in allowing initial docking of SopE/E2 to such a range of proteins, with subsequent complex stabilization by local adjustments in both SopE/E2 and GTPase/non-GTPase.

ACKNOWLEDGMENT

We thank Professor Lewis Kay (University of Toronto, Toronto, ON) for providing pulse sequences and Dr. Rieko Ishima (National Institutes of Health, Bethesda, MD) and Dr. Ranjith Muhandiram (University of Toronto) for helpful discussions.

REFERENCES

1. Hueck, C. J. (1998) Type III protein secretion systems in bacterial pathogens of animals and plants, *Microbiol. Mol. Biol. Rev. 62*, 379−433.
2. Chen, L. M., Hobbie, S., and Galán, J. E. (1996) Requirement of Cdc42 for *Salmonella*-induced cytoskeletal and nuclear responses, *Science 274*, 2115−2118.
3. Bishop, A. L., and Hall, A. (2000) Rho GTPases and their effector proteins, *Biochem. J. 348*, 241−255.
4. Cerione, R. A. (2004) Cdc42: new roads to travel, *Trends Cell Biol. 14*, 127−132.
5. Karnoub, A. E., Symons, M., Campbell, S. L., and Der, C. J. (2004) Molecular basis for rho GTPase signaling specificity, *Breast Cancer Res. Treat. 84*, 61−71.
6. Raftopoulou, M., and Hall, A. (2004) Cell migration: Rho GTPases lead the way, *Dev. Biol. 265*, 23−32.
7. Cherfils, J., and Chardin, P. (1999) GEFs: structural basis for their activation of small GTP-binding proteins, *Trends Biochem. Sci. 24*, 306−311.
8. Schmidt, A., and Hall, A. (2002) Guanine nucleotide exchange factors for Rho GTPases: turning on the switch, *Genes Dev. 16*, 1587−1609.
9. Erickson, J. W., and Cerione, R. A. (2004) Structural elements, mechanism, and evolutionary convergence of Rho protein-guanine nucleotide exchange factor complexes, *Biochemistry 43*, 837−842.
10. Cerione, R. A., and Zheng, Y. (1996) The Dbl family of oncogenes, *Curr. Opin. Cell Biol. 8*, 216−222.
11. Worthylake, D. K., Rossman, K. L., and Sondek, J. (2000) Crystal structure of Rac1 in complex with the guanine nucleotide exchange region of Tiam1, *Nature 408*, 682−688.
12. Rossman, K. L., Worthylake, D. K., Snyder, J. T., Siderovski, D. P., Campbell, S. L., and Sondek, J. (2002) A crystallographic view of interactions between Dbs and Cdc42: PH domain-assisted guanine nucleotide exchange, *EMBO J. 21*, 1315−1326.
13. Snyder, J. T., Worthylake, D. K., Rossman, K. L., Betts, L., Pruitt, W. M., Siderovski, D. P., Der, C. J., and Sondek, J. (2002) Structural basis for the selective activation of Rho GTPases by Dbl exchange factors, *Nat. Struct. Biol. 9*, 468−475.
14. Hardt, W. D., Chen, L. M., Schuebel, K. E., Bustelo, X. R., and Galán, J. E. (1998) *S. typhimurium* encodes an activator of Rho GTPases that induces membrane ruffling and nuclear responses in host cells, *Cell 93*, 815−826.
15. Bakshi, C. S., Singh, V. P., Wood, M. W., Jones, P. W., Wallis, T. S., and Galyov, E. E. (2000) Identification of SopE2, a *Salmonella* secreted protein which is highly homologous to SopE and involved in bacterial invasion of epithelial cells, *J. Bacteriol. 182*, 2341−2344.
16. Stender, S., Friebel, A., Linder, S., Rohde, M., Mirold, S., and Hardt, W. D. (2000) Identification of SopE2 from *Salmonella typhimurium*, a conserved guanine nucleotide exchange factor for Cdc42 of the host cell, *Mol. Microbiol. 36*, 1206−1221.
17. Norris, F. A., Wilson, M. P., Wallis, T. S., Galyov, E. E., and Majerus, P. W. (1998) SopB, a protein required for virulence of *Salmonella dublin*, is an inositol phosphate phosphatase, *Proc. Natl. Acad. Sci. U.S.A. 95*, 14057−14059.
18. Zhou, D. G., Chen, L. M., Hernandez, L., Shears, S. B., and Galán, J. E. (2001) A *Salmonella* inositol polyphosphatase acts in conjunction with other bacterial effectors to promote host cell actin cytoskeleton rearrangements and bacterial internalization, *Mol. Microbiol. 39*, 248−259.
19. Rudolph, M. G., Weise, C., Mirold, S., Hillenbrand, B., Bader, B., Wittinghofer, A., and Hardt, W. D. (1999) Biochemical analysis of SopE from *Salmonella typhimurium*, a highly efficient guanosine nucleotide exchange factor for RhoGTPases, *J. Biol. Chem. 274*, 30501−30509.
20. Friebel, A., Ilchmann, H., Aelpfelbacher, M., Ehrbar, K., Machleidt, W., and Hardt, W. D. (2001) SopE and SopE2 from *Salmonella typhimurium* activate different sets of RhoGTPases of the host cell, *J. Biol. Chem. 276*, 34035−34040.
21. Schlumberger, M. C., Friebel, A., Buchwald, G., Scheffzek, K., Wittinghofer, A., and Hardt, W.-D. (2003) Amino acids of the bacterial toxin SopE involved in G nucleotide exchange on Cdc42, *J. Biol. Chem. 278*, 27149−27159.
22. Stevens, M. P., Friebel, A., Taylor, L. A., Wood, M. W., Brown, P. J., Hardt, W. D., and Galyov, E. E. (2003) A *Burkholderia pseudomallei* type III secreted protein, BopE, facilitates bacterial invasion of epithelial cells and exhibits guanine nucleotide exchange factor activity, *J. Bacteriol. 185*, 4992−4996.
23. Consortium, B. N. G. P. (2003) The complete genome sequence of *Chromobacterium violaceum* reveals remarkable and exploitable bacterial adaptability, *Proc. Natl. Acad. Sci. U.S.A. 100*, 11660−11665.
24. Buchwald, G., Friebel, A., Galán, J. E., Hardt, W. D., Wittinghofer, A., and Scheffzek, K. (2002) Structural basis for the reversible activation of a Rho protein by the bacterial toxin SopE, *EMBO J. 21*, 3286−3295.
25. Mukherjee, K., Parashuraman, S., Raje, M., and Mukhopadhyay, A. (2001) SopE acts as an Rab5-specific nucleotide exchange factor and recruits non-prenylated Rab5 on *Salmonella*-containing phagosomes to promote fusion with early endosomes, *J. Biol. Chem. 276*, 23607−23615.
26. Williams, C., Galyov, E. E., and Bagby, S. (2003) Assignment of the ^{1}H, ^{13}C and ^{15}N resonances of the catalytic domain of guanine nucleotide exchange factor SopE2 from *Salmonella dublin*, *J. Biomol. NMR 26*, 379−380.
27. Delaglio, F., Grzesiek, S., Vuister, G. W., Zhu, G., Pfeifer, J., and Bax, A. (1995) NMRPipe: a multidimensional spectral processing system based on UNIX pipes, *J. Biomol. NMR 6*, 277−293.
28. Goddard, T. D., and Kneller, D. G. (1993) *Sparky: NMR assignment and integration software*, University of California, San Francisco.
29. Macura, S., and Ernst, R. R. (1980) Elucidation of cross-relaxation in liquids by two-dimensional NMR spectroscopy, *J. Phys. 41*, 95−117.
30. Zhang, O. W., Kay, L. E., Olivier, J. P., and Forman-Kay, J. D. (1994) Backbone ^{1}H and ^{15}N resonance assignments of the N-terminal SH3 domain of drk in folded and unfolded states using enhanced-sensitivity pulsed-field gradient NMR techniques, *J. Biomol. NMR 4*, 845−858.
31. Pascal, S. M., Muhandiram, D. R., Yamazaki, T., Forman-Kay, J. D., and Kay, L. E. (1994) Simultaneous acquisition of ^{15}N-edited and ^{13}C-edited NOE spectra of proteins dissolved in H_2O, *J. Magn. Reson., Ser. B 103*, 197−201.
32. Nilges, M. (1993) A calculation strategy for the structure determination of symmetrical dimers by ^{1}H NMR, *Proteins 17*, 297−309.
33. Cornilescu, G., Delaglio, F., and Bax, A. (1999) Protein backbone angle restraints from searching a database for chemical shift and sequence homology, *J. Biomol. NMR 13*, 289−302.
34. Schwieters, C. D., Kuszewski, J. J., Tjandra, N., and Clore, G. M. (2003) The Xplor-NIH NMR molecular structure determination package, *J. Magn. Reson. 160*, 65−73.
35. Schwieters, C. D., and Clore, G. M. (2001) The VMD-XPLOR visualization package for NMR structure refinement, *J. Magn. Reson. 149*, 239−244.
36. Laskowski, R. A., Rullmann, J. A. C., MacArthur, M. W., Kaptein, R., and Thornton, J. M. (1996) AQUA and PROCHECK-NMR: Programs for checking the quality of protein structures solved by NMR, *J. Biomol. NMR 8*, 477−486.
37. Koradi, R., Billeter, M., and Wuthrich, K. (1996) MOLMOL: A program for display and analysis of macromolecular structures, *J. Mol. Graphics 14*, 51−55.
38. Farrow, N. A., Muhandiram, R., Singer, A. U., Pascal, S. M., Kay, C. M., Gish, G., Shoelson, S. E., Pawson, T., Forman-Kay, J. D., and Kay, L. E. (1994) Backbone dynamics of a free and a phosphopeptide-complexed Src homology-2 domain studied by ^{15}N NMR relaxation, *Biochemistry 33*, 5984−6003.
39. Korzhnev, D. M., Skrynnikov, N. R., Millet, O., Torchia, D., and Kay, L. E. (2002) An NMR experiment for the accurate measurement of heteronuclear spin-lock relaxation rates, *J. Am. Chem. Soc. 124*, 10743−10753.
40. Kay, L. E., Torchia, D. A., and Bax, A. (1989) Backbone dynamics of proteins as studied by ^{15}N inverse detected heteronuclear NMR spectroscopy: application to staphylococcal nuclease, *Biochemistry 28*, 8972−8979.
41. Lee, L. K., Rance, M., Chazin, W. J., and Palmer, A. G. (1997) Rotational diffusion anisotropy of proteins from simultaneous analysis of ^{15}N and ^{13}Cα nuclear spin relaxation, *J. Biomol. NMR 9*, 287−298.
42. Lipari, G., and Szabo, A. (1982) Model-free approach to the interpretation of nuclear magnetic resonance relaxation in macromolecules. 1. Theory and range of validity, *J. Am. Chem. Soc. 104*, 4546−4559.

43. Clore, G. M., Szabo, A., Bax, A., Kay, L. E., Driscoll, P. C., and Gronenborn, A. M. (1990) Deviations from the simple 2-parameter model-free approach to the interpretation of ^{15}N nuclear magnetic relaxation of proteins, *J. Am. Chem. Soc. 112*, 4989−4991.
44. Dosset, P., Hus, J. C., Blackledge, M., and Marion, D. (2000) Efficient analysis of macromolecular rotational diffusion from heteronuclear relaxation data, *J. Biomol. NMR 16*, 23−28.
45. McAlister, M. S. B., Mott, H. R., van der Merwe, P. A., Campbell, I. D., Davis, S. J., and Driscoll, P. C. (1996) NMR analysis of interacting soluble forms of the cell−cell recognition molecules CD2 and CD48, *Biochemistry 35*, 5982−5991.
46. de la Torre, J. G., Huertas, M. L., and Carrasco, B. (2000) HYDRONMR: Prediction of NMR relaxation of globular proteins from atomic-level structures and hydrodynamic calculations, *J. Magn. Reson. 147*, 138−146.
47. Mandel, A. M., Akke, M., and Palmer, A. G. (1995) Backbone dynamics of *Escherichia coli* ribonuclease HI: correlations with structure and function in an active enzyme, *J. Mol. Biol. 246*, 144−163.
48. Geyer, M., Schweins, T., Herrmann, C., Prisner, T., Wittinghofer, A., and Kalbitzer, H. R. (1996) Conformational transitions in p21(ras) and in its complexes with the effector protein Raf-RBD and the GTPase activating protein GAP, *Biochemistry 35*, 10308−10320.
49. Feltham, J. L., Dötsch, V., Raza, S., Manor, D., Cerione, R. A., Sutcliffe, M. J., Wagner, G., and Oswald, R. E. (1997) Definition of the switch surface in the solution structure of Cdc42Hs, *Biochemistry 36*, 8755−8766.
50. Loh, A. P., Guo, W., Nicholson, L. K., and Oswald, R. E. (1999) Backbone dynamics of inactive, active, and effector-bound Cdc42Hs from measurements of ^{15}N relaxation parameters at multiple field strengths, *Biochemistry 38*, 12547−12557.
51. Gizachew, D., and Oswald, R. E. (2001) Concerted motion of a protein-peptide complex: backbone dynamics studies of an ^{15}N-labeled peptide derived from P^{21}-activated kinase bound to Cdc42Hs·GMPPCP, *Biochemistry 40*, 14368−14375.
52. Palmer, A. G. (2001) NMR probes of molecular dynamics: Overview and comparison with other techniques, *Annu. Rev. Biophys. Biomol. Struct. 30*, 129−155.
53. Stender, S. (2002) Identification and functional analysis of the highly conserved virulence factor SopE2 of *S. typhimurium*, Ph.D. Thesis, Technische Universität München, München, Germany.

BI0490744